Article:
Karageorghis, A. and Lesnic, D. (2025) The Method of Fundamental Solutions for Optical Fluorescence. Annals of Applied Mathematics, 41 (2). pp. 219-238. ISSN: 2096-0174

https://doi.org/10.4208/aam.OA-2025-0010

THE METHOD OF FUNDAMENTAL SOLUTIONS FOR OPTICAL FLUORESCENCE

ANDREAS KARAGEORGHIS AND DANIEL LESNIC

Abstract. In this paper, we develop the method of fundamental solutions (MFS) for solving boundary value problems in the field of optical fluorescence. The governing system of diffusion–absorption equations for the excitation and emission fluences is transformed into a single fourth–order partial differential equation whose fundamental solution can be expressed as the difference of two fundamental solutions of the complex Helmholtz equation. The numerically obtained results confirm the accuracy of the MFS when compared with an available analytical solution. Numerical results are also provided for a physical application in optical fluorescence. Furthermore, extensions to three dimensions along with numerical verification are performed.

1. Introduction

Based on the fact that near–infrared light at wavelengths between 700 to 900 nm can travel several centimeters into a biological tissue, fluorescence optical tomography has emerged as a suitable molecular imaging tool for anomaly detection, see e.g., [1, 12, 13, 14, 18]. In the iterative process of inverse retrieval of a concealed defect in a tissue, a direct solver has to be called repeatedly many times until convergence of a nonlinear minimization algorithm is achieved. Prior to this study, the finite element method (FEM) has been utilized and applied adaptively with some success [1, 11, 13, 14]. The FEM has the advantage of dealing with inhomogeneous media, but in many cases the biological properties of tissues as well as the fluorescent properties of contrasting agents employed in molecular imaging are piecewise constant across various layers of material. In these situations it is then possible to apply simpler and faster approximation methods such as the method of fundamental solutions (MFS), which is a versatile meshless boundary collocation technique for solving both direct and inverse boundary value problems [6, 16] without the need of internal domain discretisation. This method, like the boundary element method (BEM) [7, 10], is applicable to problems governed by equations, the partial differential operators of which possess explicitly available fundamental solutions.

The paper is organized as follows. In Section 2 we describe the mathematical model of optical fluorescence and the details of its approximation by the MFS are provided in Section 3. Numerical experiments are presented and analyzed in Section 4 with the three–dimensional extension provided in Section 5. Finally, Section 6 highlights the conclusions of the present study.

1991 *Mathematics Subject Classification.* Primary 65N80; Secondary 65N38.

Key words and phrases. Optical fluorescence; method of fundamental solutions; elliptic equations.

2. Mathematical model

The governing equations of photon propagation in a bounded tissue Ω, in the frequency domain, can be obtained as the scattering limit of the full radiative transfer equations [2] and are given by [1, 11]

$$-\nabla\cdot(D_{\rm x}\nabla u)+\kappa_{\rm x}\,u=0 \quad \text{in} \quad \Omega, \tag{2.1}$$

$$-\nabla\cdot(D_{\rm m}\nabla v)+\kappa_{\rm m}\,v=\beta_{\rm x}\,u \quad \text{in} \quad \Omega, \tag{2.2}$$

where u is the excitation (incident) light fluence, v is the emission (fluorescence) light fluence, $\kappa_{\rm x}$ and $\kappa_{\rm m}$ are the total photon absorption coefficients at excitation (subscript x) and emission (subscript m) wavelengths, respectively, $D_{\rm x}$ and $D_{\rm m}$ are the photon diffusion coefficients at excitation and emission wavelengths, respectively, and $\beta_{\rm x}$ is a coupling coefficient defined below in equation (2.5). The boundary conditions associated to (2.1) and (2.2) are of Robin type and given by

$$2\,D_{\rm x}\,\frac{\partial u}{\partial n}+\gamma\,u+S=0 \quad \text{on} \quad \partial\Omega, \tag{2.3}$$

$$2\,D_{\rm m}\,\frac{\partial v}{\partial n}+\gamma\,v=0 \quad \text{on} \quad \partial\Omega, \tag{2.4}$$

where $\boldsymbol{n}$ is the outward unit normal to $\partial\Omega$, γ is a constant depending on the optical refractive index mismatch at the boundary [8] and S is an excitation source.

The mathematical model given by equations (2.1)–(2.4) can be interpreted as follows [1]. The excitation fluence u is described by the diffusion–absorbtion equation (2.1) that is excited by the boundary source S in equation (2.3). On the other hand, there is no boundary source term in (2.4) for the emission fluence v. Equation (2.2) states that the fluorescence light is only produced in the interior of the imaged body Ω where the excitation (incident) fluence u is absorbed by a dye (characterized by its absorption coefficient $\mu_{\rm axf}$) and then re–emitted with probability φ and phase shift $(1-{\rm i}\,\omega\,\tau)^{-1}$, where ω is the modulation frequency of the amplitude of the incident light field and τ is the life–time of the fluorosphore (associated with first order fluorescence decay kinetics). The emission fluence v is then propagated through the tissue Ω in the same way as the excited fluence, i.e. following the diffusion–absorption process according to equation (2.2), coupled with equation (2.1) through the term

$$\beta_{\rm x}=\frac{\varphi\,\mu_{\rm axf}}{1-{\rm i}\,\omega\,\tau}\,. \tag{2.5}$$

The photon diffusion and absorption coefficients in (2.1) and (2.2) are given by [11]

$$D_{\rm x}=\frac{1}{3\,(\mu_{\rm axi}+\mu_{\rm axf}+\mu'_{\rm sx})}\,, \quad D_{\rm m}=\frac{1}{3\,(\mu_{\rm ami}+\mu_{\rm amf}+\mu'_{\rm sm})}\,, \tag{2.6}$$

$$\kappa_{\rm x}=\mu_{\rm axi}+\mu_{\rm axf}+\frac{{\rm i}\,\omega}{c}\,, \quad \kappa_{\rm m}=\mu_{\rm ami}+\mu_{\rm amf}+\frac{{\rm i}\,\omega}{c}\,, \tag{2.7}$$

where $c=3\times10^{10}$ cm/s is the speed of light, and $\mu'_{\rm sx}$, $\mu_{\rm axi}$ and $\mu_{\rm axf}$ are coefficients characterizing reduced scattering, absorption due to endogenous chromophores and absorption due to exogenous fluorosphore at the excitation wavelength. The similar coefficients $\mu'_{\rm sm}$, $\mu_{\rm ami}$ and $\mu_{\rm amf}$ correspond to the emission wavelength.

In the above model defined by equations (2.1)–(2.7), $u, v, \kappa_{\rm x}, \kappa_{\rm m}, \beta_{\rm x}$ and S are complex quantities. We also dimensionalize the space variables by a characteristic length L of Ω.

3. The method of fundamental solutions (MFS)

Assuming homogeneous media such that all properties $D_{\rm x}, D_{\rm m}, \kappa_{\rm x}, \kappa_{\rm m}$ and $\beta_{\rm x}$ are constant, equations (2.1) and (2.2) in non–dimensional form may be simplified as

$$\Delta u - \alpha_{\rm x}\, u = 0 \quad \text{in} \quad \widetilde{\Omega}, \tag{3.1}$$

$$\Delta v - \alpha_{\rm m}\, v = -B_{\rm x}\, u \quad \text{in} \quad \widetilde{\Omega}, \tag{3.2}$$

where $\widetilde{\Omega}$ denotes the non–dimensionalised solution domain, $B_{\rm x} = \beta_{\rm x} L^2/D_{\rm m}$, $\alpha_{\rm x} = \kappa_{\rm x} L^2/D_{\rm x}$ and $\alpha_{\rm m} = \kappa_{\rm m} L^2/D_{\rm m}$. We can eliminate u in the system of equations (3.1)–(3.2) by taking the Laplacian of (3.2) and using (3.1) and (3.2) to obtain

$$\Delta^2 v - \alpha_{\rm m}\, \Delta v = -B_{\rm x}\, \Delta u = -B_{\rm x}\, \alpha_{\rm x}\, u = \alpha_{\rm x}\, \Delta v - \alpha_{\rm x}\, \alpha_{\rm m}\, v \quad \text{in} \quad \widetilde{\Omega},$$

or

$$0 = \Delta^2 v - (\alpha_{\rm m} + \alpha_{\rm x})\, \Delta v + \alpha_{\rm x}\, \alpha_{\rm m}\, v = (\Delta - \alpha_{\rm x}\, \mathcal{I})\, (\Delta - \alpha_{\rm m}\, \mathcal{I})\, v \quad \text{in} \quad \widetilde{\Omega}, \tag{3.3}$$

where $\mathcal{I}$ is the identity operator.

The boundary conditions (2.3)–(2.4) in non–dimensional form are given by

$$2\, \mathcal{D}_{\rm x}\, \frac{\partial u}{\partial n} + \gamma\, u + S = 0 \quad \text{on} \quad \partial\widetilde{\Omega}, \tag{3.4}$$

$$2\, \mathcal{D}_{\rm m}\, \frac{\partial v}{\partial n} + \gamma\, v = 0 \quad \text{on} \quad \partial\widetilde{\Omega}, \tag{3.5}$$

where $\mathcal{D}_{\rm x} = D_{\rm x}/L$ and $\mathcal{D}_{\rm m} = D_{\rm m}/L$. Also, from (3.4) and (3.2), eliminating u, we obtain

$$2\, \mathcal{D}_{\rm x}\, \frac{\partial}{\partial n}\, (\Delta v - \alpha_{\rm m}\, v) + \gamma\, (\Delta v - \alpha_{\rm m}\, v) - S\, B_{\rm x} = 0 \quad \text{on}\ \partial\widetilde{\Omega}. \tag{3.6}$$

Boundary value problem (3.1), (3.2), (3.4) and (3.5) has therefore been reduced to (3.3), (3.5) and (3.6). Equation (3.3) is a fourth–order partial differential equation (PDE) and the boundary conditions (3.5) and (3.6) involve all the primary and secondary variables $v, \partial v/\partial n, \Delta v$ and $\partial(\Delta v)/\partial n$. Various meshless methods [4, 19, 20] can be employed for solving boundary value problem (3.3), (3.5) and (3.6).

We may rewrite the fourth–order equation (3.3) as a system of two second–order complex Helmholtz equations

$$\Delta v - \alpha_{\rm m} v = w \quad \text{in}\ \widetilde{\Omega}, \tag{3.7}$$

$$\Delta w - \alpha_{\rm x} w = 0 \quad \text{in}\ \widetilde{\Omega}. \tag{3.8}$$

Equation (3.7) is subjected to the Robin boundary condition (3.5), whilst for equation (3.8), equation (3.6) implies the Robin boundary condition

$$2\, \frac{\partial w}{\partial n} + \gamma\, w = S\, B_{\rm x} \quad \text{on} \quad \partial\widetilde{\Omega}. \tag{3.9}$$

We may therefore first solve (3.8) and (3.9) to obtain w in $\widetilde{\Omega}$, after which we can solve the inhomogeneous equation (3.7) subject to (3.5) to determine v in $\widetilde{\Omega}$. Alternatively, we may solve the fourth–order PDE (3.3) directly without the splitting (3.7)–(3.8) by remarking that a particular solution to (3.3) can be written as the difference

$$v = \frac{\Phi_{\mathrm{m}} - \Phi_{\mathrm{x}}}{\alpha_{\mathrm{m}} - \alpha_{\mathrm{x}}}\,, \tag{3.10}$$

where Φ_{m} and Φ_{x} are particular solutions to the second-order complex Helmholtz equations

$$\Delta\Phi_{\mathrm{m}} - \alpha_{\mathrm{m}}\,\Phi_{\mathrm{m}} = 0 \quad \text{and} \quad \Delta\Phi_{\mathrm{x}} - \alpha_{\mathrm{x}}\,\Phi_{\mathrm{x}} = 0\,, \tag{3.11}$$

see [19]. Applying the Laplacian operator to (3.10) and using (3.11) we remark that

$$\Delta v = \frac{\alpha_{\mathrm{m}}\,\Phi_{\mathrm{m}} - \alpha_{\mathrm{x}}\,\Phi_{\mathrm{x}}}{\alpha_{\mathrm{m}} - \alpha_{\mathrm{x}}}\,, \tag{3.12}$$

which gives an effective way of computing the Laplacian of v needed in (3.6). Moreover, $\partial v/\partial n$ and $\partial(\Delta v)/\partial n$ may be obtained by taking the normal derivatives of (3.10) and (3.12), respectively.

3.1. The MFS for finding the excitation fluence u satisfying equations (3.1) and (3.4).

The fundamental solution of the complex Helmholtz equation

$$\Delta\Phi - \alpha\,\Phi = 0, \tag{3.13}$$

with $\alpha \in \mathbb{C}$, in two dimensions is given by [9]:

$$\Phi(\boldsymbol{x};\boldsymbol{\xi}) = -\frac{1}{2\pi} K_0\left(\sqrt{\alpha}\,|\boldsymbol{x}-\boldsymbol{\xi}|\right), \tag{3.14}$$

where K_0 is the modified Bessel function of the second kind of order zero and, for $\alpha = a + \mathrm{i}b$, we take

$$\sqrt{\alpha} = \sqrt{\frac{a+\sqrt{a^2+b^2}}{2}} + \mathrm{i}\,\frac{b}{|b|}\sqrt{\frac{-a+\sqrt{a^2+b^2}}{2}}\,.$$

In the MFS, we approximate the solution of (3.1) and (3.4) by a linear combination of non–singular fundamental solutions of the form (3.14), namely,

$$u_N(\boldsymbol{x}) = -\frac{1}{2\pi}\sum_{j=1}^{N} c_j\,K_0\left(\sqrt{\alpha_{\mathrm{x}}}\,|\boldsymbol{x}-\boldsymbol{\xi}_j|\right), \quad \boldsymbol{x} \in \widetilde{\Omega} \cup \partial\widetilde{\Omega}, \tag{3.15}$$

where $\left(\boldsymbol{\xi}_j\right)_{j=\overline{1,N}}$ are source points located outside $\widetilde{\Omega} \cup \partial\widetilde{\Omega}$ (such that u_N satisfies PDE (3.1) in $\widetilde{\Omega}$) and $(c_j)_{j=\overline{1,N}}$ are unknown complex coefficients to be determined by imposing the boundary condition (3.4). In doing so, we also require the normal derivative of u_N, which, from (3.15), can be approximated as:

$$\frac{\partial u_N}{\partial n}(\boldsymbol{x}) = \frac{\sqrt{\alpha_{\mathrm{x}}}}{2\pi}\sum_{j=1}^{N} c_j\,K_1\left(\sqrt{\alpha_{\mathrm{x}}}\,|\boldsymbol{x}-\boldsymbol{\xi}_j|\right)\frac{(\boldsymbol{x}-\boldsymbol{\xi}_j)\cdot\boldsymbol{n}(\boldsymbol{x})}{|\boldsymbol{x}-\boldsymbol{\xi}_j|}\,, \quad \boldsymbol{x} \in \partial\widetilde{\Omega}, \tag{3.16}$$

where $K_1 = -K_0'$ is the modified Bessel function of the second kind of order one.

The boundary condition (3.4) is imposed at $(\boldsymbol{x}_k)_{k=\overline{1,M}}$ points uniformly distributed over the boundary $\partial\widetilde{\Omega}$ yielding the following system of M complex equations in the $(c_j)_{j=\overline{1,N}}$ complex unknowns:

$$2\,\mathcal{D}_x \frac{\partial u_N}{\partial n}(\boldsymbol{x}_k) + \gamma\, u_N(\boldsymbol{x}_k) = -S(\boldsymbol{x}_k), \quad k = \overline{1,M}, \tag{3.17}$$

Remark 1. The source points $\left(\boldsymbol{\xi}_j\right)_{j=\overline{1,N}}$ are generated as follows. We first distribute the points $\left(\tilde{\boldsymbol{\xi}}_j\right)_{j=\overline{1,N}}$ uniformly around the boundary $\partial\widetilde{\Omega}$ and then take

$$\boldsymbol{\xi}_j = \mathbf{x}_{\rm c} + \eta\left(\tilde{\boldsymbol{\xi}}_j - \mathbf{x}_{\rm c}\right), \quad j = \overline{1,N}, \tag{3.18}$$

where $\mathbf{x}_{\rm c}$ is the centroid of $\widetilde{\Omega}$ and $\eta > 1$ is an appropriately chosen dilation parameter.

3.2. **The MFS for finding the emission fluence v satisfying equations** (3.3)**,** (3.5) **and** (3.6)**.** According to (3.10) we obtain that the fundamental solution of the fourth–order PDE (3.3) in two dimensions is given by

$$V(\boldsymbol{x};\boldsymbol{\xi}) = -\frac{1}{2\pi(\alpha_{\rm m}-\alpha_{\rm x})}\left[K_0\left(\sqrt{\alpha_{\rm m}}\,|\boldsymbol{x}-\boldsymbol{\xi}|\right) - K_0\left(\sqrt{\alpha_{\rm x}}\,|\boldsymbol{x}-\boldsymbol{\xi}|\right)\right]. \tag{3.19}$$

In the MFS, we approximate the solution to (3.3), (3.5) and (3.6) by a linear combination of non–singular fundamental solutions (3.19) in the form

$$v_N(\boldsymbol{x}) = \sum_{j=1}^{2N} d_j\, V(\boldsymbol{x};\boldsymbol{\xi}_j)$$

$$= -\frac{1}{2\pi(\alpha_{\rm m}-\alpha_{\rm x})}\sum_{j=1}^{2N} d_j\left[K_0\left(\sqrt{\alpha_{\rm m}}\,|\boldsymbol{x}-\boldsymbol{\xi}_j|\right) - K_0\left(\sqrt{\alpha_{\rm x}}\,|\boldsymbol{x}-\boldsymbol{\xi}_j|\right)\right], \quad \boldsymbol{x}\in\widetilde{\Omega}\cup\partial\widetilde{\Omega}, \tag{3.20}$$

where $\left(\boldsymbol{\xi}_j\right)_{j=\overline{1,2N}}$ are source points located outside $\widetilde{\Omega}\cup\partial\widetilde{\Omega}$ (such that v_N satisfies the PDE (3.3) in $\widetilde{\Omega}$) and $(d_j)_{j=\overline{1,2N}}$ are unknown complex coefficients to be determined by imposing the boundary conditions (3.5) and (3.6). In doing so, we also need the derivatives of v_N, which from (3.20) can be approximated as (see also (3.12)):

$$\frac{\partial v_N}{\partial n}(\boldsymbol{x}) = \sum_{j=1}^{2N} d_j\,\frac{\partial V}{\partial n}(\boldsymbol{x};\boldsymbol{\xi}_j) = \frac{1}{2\pi(\alpha_{\rm m}-\alpha_{\rm x})}\sum_{j=1}^{2N} d_j\,\left[\sqrt{\alpha_{\rm m}}\,K_1\left(\sqrt{\alpha_{\rm m}}\,|\boldsymbol{x}-\boldsymbol{\xi}_j|\right)\right.$$

$$\left. -\sqrt{\alpha_{\rm x}}\,K_1\left(\sqrt{\alpha_{\rm x}}\,|\boldsymbol{x}-\boldsymbol{\xi}_j|\right)\right]\frac{(\boldsymbol{x}-\boldsymbol{\xi}_j)\cdot\boldsymbol{n}(\boldsymbol{x})}{|\boldsymbol{x}-\boldsymbol{\xi}_j|}, \quad \boldsymbol{x}\in\partial\widetilde{\Omega}, \tag{3.21}$$

$$\Delta v_N(\boldsymbol{x}) = \sum_{j=1}^{2N} d_j\,\Delta V(\boldsymbol{x};\boldsymbol{\xi}_j)$$

$$= -\frac{1}{2\pi(\alpha_{\mathrm{m}}-\alpha_{\mathrm{x}})} \sum_{j=1}^{2N} d_j \left[\alpha_{\mathrm{m}} K_0\left(\sqrt{\alpha_{\mathrm{m}}}\,|\boldsymbol{x}-\boldsymbol{\xi}_j|\right) - \alpha_{\mathrm{x}}\, K_0\left(\sqrt{\alpha_{\mathrm{x}}}\,|\boldsymbol{x}-\boldsymbol{\xi}_j|\right)\right], \quad \boldsymbol{x} \in \widetilde{\Omega} \cup \partial\widetilde{\Omega}, \quad (3.22)$$

$$\frac{\partial(\Delta v_N)}{\partial n}(\boldsymbol{x}) = \sum_{j=1}^{2N} d_j \frac{\partial(\Delta V)}{\partial n}(\boldsymbol{x};\boldsymbol{\xi}_j) = \frac{1}{2\pi(\alpha_{\mathrm{m}}-\alpha_x)} \sum_{j=1}^{2N} d_j \left[\alpha_{\mathrm{m}}^{3/2} K_1\left(\sqrt{\alpha_{\mathrm{m}}}\,|\boldsymbol{x}-\boldsymbol{\xi}_j|\right)\right.$$

$$\left. -\alpha_{\mathrm{x}}^{3/2} K_1\left(\sqrt{\alpha_{\mathrm{x}}}\,|\boldsymbol{x}-\boldsymbol{\xi}_j|\right)\right] \frac{(\boldsymbol{x}-\boldsymbol{\xi}_j)\cdot\boldsymbol{n}(\boldsymbol{x})}{|\boldsymbol{x}-\boldsymbol{\xi}_j|}, \quad \boldsymbol{x} \in \partial\widetilde{\Omega}. \quad (3.23)$$

The boundary conditions (3.5) and (3.6) are imposed at the points $(\boldsymbol{x}_k)_{k=\overline{1,M}}$ resulting in the following system of $2M$ complex equations in the $(d_j)_{j=\overline{1,2N}}$ complex unknowns:

$$2\,\mathcal{D}_{\mathrm{m}} \frac{\partial v_N}{\partial n}(\boldsymbol{x}_k) + \gamma\, v_N(\boldsymbol{x}_k) = 0 \quad k = \overline{1,M}, \quad (3.24)$$

$$2\,\mathcal{D}_{\mathrm{x}} \frac{\partial(\Delta v_N)}{\partial n}(\boldsymbol{x}_k) - 2\,\mathcal{D}_{\mathrm{x}}\,\alpha_{\mathrm{m}} \frac{\partial v_N}{\partial n}(\boldsymbol{x}_k) + \gamma\,\Delta v_N(\boldsymbol{x}_k) - \gamma\,\alpha_{\mathrm{m}}\, v_N(\boldsymbol{x}_k) = B_{\mathrm{x}}\, S(\boldsymbol{x}_k), \quad k = \overline{1,M}. \quad (3.25)$$

Remark 2. Following the ideas developed for polyharmonic boundary value problems in [15], the source points $\left(\boldsymbol{\xi}_j\right)_{j=\overline{1,2N}}$ are now generated as follows. As in (3.18), we first distribute the points $\left(\tilde{\boldsymbol{\xi}}_j\right)_{j=\overline{1,2N}}$ uniformly around the boundary $\partial\tilde{\Omega}$ and then distribute the sources on two pseudo–boundaries as follows:

$$\boldsymbol{\xi}_{(\ell-1)N+j} = \mathrm{x}_{\mathrm{c}} + \eta_\ell\left(\tilde{\boldsymbol{\xi}}_j - \mathrm{x}_{\mathrm{c}}\right), \quad j = \overline{1,N},\ \ell = 1,2, \quad (3.26)$$

where η_ℓ, $\ell = 1,2$, are appropriately chosen dilation parameters with $\eta_2 > \eta_1 > 1$.

4. NUMERICAL EXPERIMENTS

Mimicking previous experiments [11, 12, 13, 14], two–dimensional phantom numerical experiments for optical fluorescence are considered using a $(0,L)\times(0,L) = \Omega$ acrylic square plate with $L = 8$ cm filled with 1% liposyn solution containing 1μ M indocyamine green (ICG) dye. This dye has the quantum efficiency and the lifetime of fluorophore equal to $\varphi = 0.016$ and $\tau = 0.56 \times 10^{-9}$ s, respectively, [11]. The excitation wavelength of the ICG dye is 785 nm modulated at ω =100MHz=10^8 s^{-1} and the emission wavelength is 830 nm, according to the literature. The index mismatch parameter at the boundary $\partial\Omega$ between the acrylic plate and the phontom is given by $\gamma = 1/1.0454 = 0.9566$, see [8]. The scattering and absorption coefficients characteristic to the 1% liposyn solution are [11]

$$\mu'_{\mathrm{sx}} = \mu'_{\mathrm{sm}} = 9.84\,\mathrm{cm}^{-1},$$

$$\mu_{\mathrm{ami}} = 0.0289\,\mathrm{cm}^{-1}, \quad \mu_{\mathrm{axi}} = 0.023\,\mathrm{cm}^{-1},$$

$$\mu_{\mathrm{amf}} = 0.00506\,\mathrm{cm}^{-1}, \quad \mu_{\mathrm{axf}} = 0.005\,\mathrm{cm}^{-1},$$

which are similar to the optical properties of the human breast tissue. The above data on the physical quantities L, φ, τ, ω, γ, μ'_{sx}, μ'_{sm}, μ_{ami}, μ_{axi}, μ_{amf} and μ_{axf} introduced into (2.5)–(2.7) yield $\widetilde{\Omega} = (0,1) \times (0,1)$ and

$$\beta_{\mathrm{x}} = \frac{\varphi\, \mu_{\mathrm{axf}}}{1 - \mathrm{i}\, \omega\, \tau} = \frac{0.016 \times 0.005}{1 - \mathrm{i} \times 0.59 \times 10^{-9} \times 10^{8}} = \frac{8 \times 10^{-5} \times (1 + 0.056\, \mathrm{i})}{1.001566773}\, \mathrm{cm}^{-1},$$

$$D_{\mathrm{x}} = \frac{1}{3\,(\mu_{\mathrm{axi}} + \mu_{\mathrm{axf}} + \mu'_{\mathrm{sx}})} = \frac{1}{3\,(0.023 + 0.005 + 9.84)} = 0.03378\, \mathrm{cm},$$

$$D_{\mathrm{m}} = \frac{1}{3\,(\mu_{\mathrm{ami}} + \mu_{\mathrm{amf}} + \mu'_{\mathrm{sm}})} = \frac{1}{3\,(0.0289 + 0.00506 + 9.84)} = 0.03376\, \mathrm{cm},$$

$$\kappa_{\mathrm{x}} = \mu_{\mathrm{axi}} + \mu_{\mathrm{axf}} + \frac{\mathrm{i}\, \omega}{c} = 0.023 + 0.005 + \frac{\mathrm{i} \times 10^{8}}{3 \times 10^{10}} = (0.0280 + 0.0033\, \mathrm{i})\ \mathrm{cm}^{-1},$$

$$\kappa_{\mathrm{m}} = \mu_{\mathrm{ami}} + \mu_{\mathrm{amf}} + \frac{\mathrm{i}\, \omega}{c} = 0.0289 + 0.00506 + \frac{\mathrm{i} \times 10^{8}}{3 \times 10^{10}} = (0.03396 + 0.0033\, \mathrm{i})\ \mathrm{cm}^{-1}.$$

Furthermore, in (3.1), (3.2), (3.5) and (3.9) we need the non–dimensional quantities $\widetilde{\Omega} = (0,1) \times (0,1)$ and

$$\alpha_{\mathrm{x}} = \frac{\kappa_{\mathrm{x}}\, L^2}{D_{\mathrm{x}}} = \frac{64\,(0.0280 + 0.0033\, \mathrm{i})}{0.03377921902} = 53.0503 + 6.3092\, \mathrm{i},$$

$$\alpha_{\mathrm{m}} = \frac{\kappa_{\mathrm{m}}\, L^2}{D_{\mathrm{m}}} = \frac{64\,(0.03396 + 0.0033\, \mathrm{i})}{0.03375882962} = 64.3813 + 6.3030\, \mathrm{i},$$

$$B_{\mathrm{x}} = \frac{\beta_{\mathrm{x}}\, L^2}{D_{\mathrm{m}}} = \frac{64 \times 8 \times 10^{-5}\,(1 + 0.056\, \mathrm{i})}{1.001566773 \times 0.03375882962} = 0.1514 + 8.48 \times 10^{-3}\, \mathrm{i},$$

$$\mathcal{D}_{\mathrm{x}} = \frac{D_{\mathrm{x}}}{L} = \frac{0.03377921902}{8} = 4.222 \times 10^{-3},$$

$$\mathcal{D}_{\mathrm{m}} = \frac{D_{\mathrm{m}}}{L} = \frac{0.03375882962}{8} = 4.2198 \times 10^{-3}.$$

We also illuminate the top boundary $y = 1$ by a Gaussian source such that in (3.6) we input

$$S(x,y) = \begin{cases} \dfrac{1}{\sigma\sqrt{2\pi}}\, \exp\left(-\dfrac{(x-\nu)^2}{2\sigma^2}\right) & \text{on } y = 1,\ x \in (0,1), \\[2ex] 0 & \text{elsewhere on } \partial\widetilde{\Omega}, \end{cases} \tag{4.1}$$

where $\nu = 0.5$ is the mean and $\sigma = 0.1$ is the standard deviation.

4.1. **Verification of the numerical code.** Before attempting to solve the direct problems given by equations (3.1) and (3.4) for u, and by equations (3.3), (3.5) and (3.6) for v, which do not have a readily available simple explicit exact solution, we verify the numerical code on fabricated analytical solutions given by

$$u(\boldsymbol{x}) = -\frac{1}{2\pi} K_0 \left(\sqrt{\alpha_{\mathrm{x}}}\, |\boldsymbol{x} - \boldsymbol{\xi}^*| \right), \quad \boldsymbol{x} \in \widetilde{\Omega} \cup \partial\widetilde{\Omega}, \tag{4.2}$$

and

$$v(\boldsymbol{x}) = V(\boldsymbol{x}; \boldsymbol{\xi}^*), \quad \boldsymbol{x} \in \widetilde{\Omega} \cup \partial\widetilde{\Omega}, \tag{4.3}$$

where $\boldsymbol{\xi}^* = (3, 0)$ is well–outside the solution domain $\widetilde{\Omega} = (0, 1) \times (0, 1)$.

The function defined in equation (4.2) satisfies the PDE (3.1) and the inhomogeneous boundary conditions

$$\begin{aligned} &2\,\mathcal{D}_{\mathrm{x}} \frac{\partial u}{\partial n}(\boldsymbol{x}) + \gamma\, u(\boldsymbol{x}) \\ &= \frac{\mathcal{D}_{\mathrm{x}} \sqrt{\alpha_{\mathrm{x}}}}{\pi} K_1 \left(\sqrt{\alpha_{\mathrm{x}}}\, |\boldsymbol{x} - \boldsymbol{\xi}^*| \right) \frac{(\boldsymbol{x} - \boldsymbol{\xi}_j) \cdot \boldsymbol{n}(\boldsymbol{x})}{|\boldsymbol{x} - \boldsymbol{\xi}_j|} - \frac{\gamma}{2\pi} K_0 \left(\sqrt{\alpha_{\mathrm{x}}}\, |\boldsymbol{x} - \boldsymbol{\xi}^*| \right) =: R(\boldsymbol{x}), \quad \boldsymbol{x} \in \partial\widetilde{\Omega}. \end{aligned} \tag{4.4}$$

Imposing this boundary condition at $(\boldsymbol{x}_k)_{k=\overline{1,M}}$ points uniformly distributed over the boundary $\partial\widetilde{\Omega}$ results in the following linear system of M complex equations in the complex unknowns $(c_j)_{j=\overline{1,N}}$:

$$2\,\mathcal{D}_{\mathrm{x}} \frac{\partial u_N}{\partial n}(\boldsymbol{x}_k) + \gamma\, u_N(\boldsymbol{x}_k) = R(\boldsymbol{x}_k), \quad k = \overline{1, M}, \tag{4.5}$$

where u_N is given by equation (3.15) with the source points $\left(\boldsymbol{\xi}_j\right)_{j=\overline{1,N}}$ placed according to (3.18).

Also, the function defined in equation (4.3) satisfies the PDE (3.3) and the inhomogeneous boundary conditions

$$2\,\mathcal{D}_{\mathrm{m}} \frac{\partial v}{\partial n}(\boldsymbol{x}) + \gamma\, v(\boldsymbol{x}) = 2\,\mathcal{D}_{\mathrm{m}} \frac{\partial V}{\partial n}(\boldsymbol{x}; \boldsymbol{\xi}^*) + \gamma\, V(\boldsymbol{x}; \boldsymbol{\xi}^*) =: R_1(\boldsymbol{x}), \quad \boldsymbol{x} \in \partial\widetilde{\Omega} \tag{4.6}$$

and

$$\begin{aligned} 2\,\mathcal{D}_{\mathrm{x}} \frac{\partial(\Delta v)}{\partial n}(\boldsymbol{x}) - 2\,\mathcal{D}_{\mathrm{x}}\, \alpha_{\mathrm{m}} \frac{\partial v}{\partial n}(\boldsymbol{x}) + \gamma\, \Delta v(\boldsymbol{x}) - \gamma\, \alpha_{\mathrm{m}}\, v(\boldsymbol{x}) = 2\,\mathcal{D}_{\mathrm{x}} \frac{\partial(\Delta V)}{\partial n}(\boldsymbol{x}; \boldsymbol{\xi}^*) \\ -2\,\mathcal{D}_{\mathrm{x}}\, \alpha_{\mathrm{m}} \frac{\partial V}{\partial n}(\boldsymbol{x}; \boldsymbol{\xi}^*) + \gamma\, \Delta V(\boldsymbol{x}; \boldsymbol{\xi}^*) - \gamma\, \alpha_{\mathrm{m}}\, V(\boldsymbol{x}; \boldsymbol{\xi}^*) =: R_2(\boldsymbol{x}), \quad \boldsymbol{x} \in \partial\widetilde{\Omega}. \end{aligned} \tag{4.7}$$

Imposing the boundary conditions (3.5) and (3.6) at the points $(\boldsymbol{x}_k)_{k=\overline{1,M}}$ results in the following linear system of $2M$ complex equations in the complex unknowns $(d_j)_{j=\overline{1,2N}}$:

$$2\,\mathcal{D}_{\mathrm{m}} \frac{\partial v_N}{\partial n}(\boldsymbol{x}_k) + \gamma\, v_N(\boldsymbol{x}_k) = R_1(\boldsymbol{x}_k), \quad k = \overline{1, M}, \tag{4.8}$$

$$2\,\mathcal{D}_{\mathrm{x}} \frac{\partial(\Delta v_N)}{\partial n}(\boldsymbol{x}_k) - 2\,\mathcal{D}_{\mathrm{x}}\, \alpha_{\mathrm{m}} \frac{\partial v_N}{\partial n}(\boldsymbol{x}_k) + \gamma\, \Delta v_N(\boldsymbol{x}_k) - \gamma\, \alpha_{\mathrm{m}}\, v_N(\boldsymbol{x}_k) = R_2(\boldsymbol{x}_k), \quad k = \overline{1, M}, \tag{4.9}$$

where v_N is given by equation (3.20) with the source points $\left(\boldsymbol{\xi}_j\right)_{j=\overline{1,2N}}$ distributed according to (3.26).

We calculated the approximations and the exact solutions on a uniform 21×21 grid in $\widetilde{\Omega} \cup \partial\widetilde{\Omega}$. We the calculated the maximum relative errors

$$E_u = \frac{|u_N - u|_\infty}{|u|_\infty}, \quad E_v = \frac{|v_N - v|_\infty}{|v|_\infty}, \text{ where } |w|_\infty = \max_{\boldsymbol{x} \in \widetilde{\Omega} \cup \partial\widetilde{\Omega}} |w(\boldsymbol{x})|, \tag{4.10}$$

for varying $\eta = \eta_1 = 1 + k/30$, $\eta_2 = 1 + k/25$, $k = \overline{1, 49}$ taking $M = N = 16, 32, 64$ and 128. The corresponding plots are given in Figure 1. From this figure it can be observed that the maximum errors (4.10) decrease as the number of degrees of freedom $M = N$ increases indicating the convergence of the MFS employed. Moreover, for the various values of the parameters $\eta = \eta_1$ and η_2, determining the distance between the two pseudo–boundaries and the boundary $\partial\widetilde{\Omega}$, the errors tend to decrease as this distance increases, but start to increase once the sources get closer to the singularity $\boldsymbol{\xi}^* = (3, 0)$ in (4.2) and (4.3).

Figures 2 and 3 show the numerical solution for the real and imaginary parts of $u(x, 1)$ and $v(x, 1)$, $x \in [0, 1]$, obtained using the MFS with $M = N = 128$, $\eta = \eta_1 = 2$, $\eta_2 = 2.2$, in comparison with the exact solutions derived from (4.2) and (4.3). From Figures 2 and 3, excellent agreement between the numerical and exact solutions can be observed.

4.2. **Application to the physical problem.**

Once the numerical method has been verified for accuracy, the physical problem given by equations (3.1) and (3.4) for u, and by equations (3.3), (3.5) and (3.6) for v can be solved by replacing in the code $R(\boldsymbol{x})$ (previously given by (4.4)) by $-S(\boldsymbol{x})$, and $R_1(\boldsymbol{x})$ and $R_2(\boldsymbol{x})$ (previously given by (4.6) and (4.7)) by 0 and $B_x S(\boldsymbol{x})$ for $\boldsymbol{x} \in \partial\widetilde{\Omega}$, respectively. In Figure 4 we present the real and imaginary parts of the approximation u_N on the top boundary while in Figure 5 we present the contours of the real and imaginary parts of the approximation for u_N with $(x, y) \in \widetilde{\Omega} \cup \partial\widetilde{\Omega} = [0, 1] \times [0, 1]$. The corresponding results for v_N are presented in Figures 6 and 7. These results were generated with $M = N = 32$, $\eta = \eta_1 = 1.2$, $\eta_2 = 1.6$.

5. EXTENSION TO THREE DIMENSIONS

In three dimensions, the fundamental solution of the complex Helmholtz equation (3.13) is given by [17]

$$\Phi(\boldsymbol{x}; \boldsymbol{\xi}) = \frac{1}{4\pi} \frac{\exp\left(-\sqrt{\alpha}\, |\boldsymbol{x} - \boldsymbol{\xi}|\right)}{|\boldsymbol{x} - \boldsymbol{\xi}|}\,, \tag{5.1}$$

and, as a result, approximations (3.15) and (3.16) become

$$u_N(\boldsymbol{x}) = \frac{1}{4\pi} \sum_{j=1}^{N} c_j \, \frac{\exp\left(-\sqrt{\alpha_{\mathrm{x}}}\, |\boldsymbol{x} - \boldsymbol{\xi}_j|\right)}{|\boldsymbol{x} - \boldsymbol{\xi}_j|}, \quad \boldsymbol{x} \in \widetilde{\Omega} \cup \partial\widetilde{\Omega}, \tag{5.2}$$

$$\frac{\partial u_N}{\partial n}(\boldsymbol{x}) = -\frac{1}{4\pi} \sum_{j=1}^{N} c_j \, \exp\left(-\sqrt{\alpha_{\mathrm{x}}}\, |\boldsymbol{x} - \boldsymbol{\xi}_j|\right) \left[1 + \sqrt{\alpha_{\mathrm{x}}} |\boldsymbol{x} - \boldsymbol{\xi}_j|\right] \frac{(\boldsymbol{x} - \boldsymbol{\xi}_j) \cdot \boldsymbol{n}(\boldsymbol{x})}{|\boldsymbol{x} - \boldsymbol{\xi}_j|^3}\,, \quad \boldsymbol{x} \in \partial\widetilde{\Omega}. \tag{5.3}$$

Also, in three dimensions, the fundamental solutions of the fourth–order PDE (3.3) is given by

$$V(\boldsymbol{x};\boldsymbol{\xi}) = \frac{1}{4\pi(\alpha_{\mathrm{m}}-\alpha_{\mathrm{x}})} \, \frac{\left[\exp\left(-\sqrt{\alpha_{\mathrm{m}}}\,|\boldsymbol{x}-\boldsymbol{\xi}|\right) - \exp\left(-\sqrt{\alpha_{\mathrm{x}}}\,|\boldsymbol{x}-\boldsymbol{\xi}|\right)\right]}{|\boldsymbol{x}-\boldsymbol{\xi}|}. \tag{5.4}$$

Consequently, approximations (3.20)–(3.23) become

$$v_N(\boldsymbol{x}) = \sum_{j=1}^{2N} d_j \, V(\boldsymbol{x};\boldsymbol{\xi}_j)$$

$$= \frac{1}{4\pi(\alpha_{\mathrm{m}}-\alpha_{\mathrm{x}})} \sum_{j=1}^{2N} d_j \frac{\left[\exp\left(-\sqrt{\alpha_{\mathrm{m}}}\,|\boldsymbol{x}-\boldsymbol{\xi}_j|\right) - \exp\left(-\sqrt{\alpha_{\mathrm{x}}}\,|\boldsymbol{x}-\boldsymbol{\xi}_j|\right)\right]}{|\boldsymbol{x}-\boldsymbol{\xi}_j|}, \quad \boldsymbol{x} \in \widetilde{\Omega} \cup \partial\widetilde{\Omega}, \tag{5.5}$$

$$\frac{\partial v_N}{\partial n}(\boldsymbol{x}) = \sum_{j=1}^{2N} d_j \, \frac{\partial V}{\partial n}(\boldsymbol{x};\boldsymbol{\xi}_j)$$

$$= -\frac{1}{4\pi(\alpha_{\mathrm{m}}-\alpha_{\mathrm{x}})} \sum_{j=1}^{2N} d_j \, \Big[\exp\left(-\sqrt{\alpha_{\mathrm{m}}}\,|\boldsymbol{x}-\boldsymbol{\xi}_j|\right) \left[1+\sqrt{\alpha_{\mathrm{m}}}\,|\boldsymbol{x}-\boldsymbol{\xi}_j|\right]$$

$$- \exp\left(-\sqrt{\alpha_{\mathrm{x}}}\,|\boldsymbol{x}-\boldsymbol{\xi}_j|\right) \left[1+\sqrt{\alpha_{\mathrm{x}}}\,|\boldsymbol{x}-\boldsymbol{\xi}_j|\right]\Big] \, \frac{(\boldsymbol{x}-\boldsymbol{\xi}_j)\cdot\boldsymbol{n}(\boldsymbol{x})}{|\boldsymbol{x}-\boldsymbol{\xi}_j|^3}, \quad \boldsymbol{x} \in \partial\widetilde{\Omega}, \tag{5.6}$$

$$\Delta v_N(\boldsymbol{x}) = \sum_{j=1}^{2N} d_j \, \Delta V(\boldsymbol{x};\boldsymbol{\xi}_j)$$

$$= \frac{1}{4\pi(\alpha_{\mathrm{m}}-\alpha_{\mathrm{x}})} \sum_{j=1}^{2N} d_j \, \frac{\left[\alpha_{\mathrm{m}} \exp\left(-\sqrt{\alpha_{\mathrm{m}}}\,|\boldsymbol{x}-\boldsymbol{\xi}_j|\right) - \alpha_{\mathrm{x}} \exp\left(-\sqrt{\alpha_{\mathrm{x}}}\,|\boldsymbol{x}-\boldsymbol{\xi}_j|\right)\right]}{|\boldsymbol{x}-\boldsymbol{\xi}_j|},$$

$$\boldsymbol{x} \in \widetilde{\Omega} \cup \partial\widetilde{\Omega}, \tag{5.7}$$

$$\frac{\partial(\Delta v_N)}{\partial n}(\boldsymbol{x}) = \sum_{j=1}^{2N} d_j \, \frac{\partial(\Delta V)}{\partial n}(\boldsymbol{x};\boldsymbol{\xi}_j)$$

$$= -\frac{1}{4\pi(\alpha_{\mathrm{m}}-\alpha_{\mathrm{x}})} \sum_{j=1}^{2N} d_j \, \Big[\alpha_{\mathrm{m}} \exp\left(-\sqrt{\alpha_{\mathrm{m}}}\,|\boldsymbol{x}-\boldsymbol{\xi}_j|\right) \left[1+\sqrt{\alpha_{\mathrm{m}}}\,|\boldsymbol{x}-\boldsymbol{\xi}_j|\right]$$

$$-\alpha_{\mathrm{x}} \exp\left(-\sqrt{\alpha_{\mathrm{x}}}\,|\boldsymbol{x}-\boldsymbol{\xi}_j|\right) \left[1+\sqrt{\alpha_{\mathrm{x}}}\,|\boldsymbol{x}-\boldsymbol{\xi}_j|\right]\Big] \, \frac{(\boldsymbol{x}-\boldsymbol{\xi}_j)\cdot\boldsymbol{n}(\boldsymbol{x})}{|\boldsymbol{x}-\boldsymbol{\xi}_j|^3}, \quad \boldsymbol{x} \in \partial\widetilde{\Omega}. \tag{5.8}$$

Note that in three dimensions, Remarks 1 and 2 on the placement of source points still apply.

5.1. **Verification of the numerical code.** We consider the solution of boundary value problems (3.1) and (3.4) for u, and (3.3), (3.5) and (3.6) for v for the analytical solutions given by

$$u(\boldsymbol{x}) = \frac{1}{4\pi}\,\frac{\exp\left(-\sqrt{\alpha_{\mathrm{x}}}\,|\boldsymbol{x}-\boldsymbol{\xi}^*|\right)}{|\boldsymbol{x}-\boldsymbol{\xi}^*|}\,, \quad \boldsymbol{x} \in \widetilde{\Omega} \cup \partial\widetilde{\Omega}, \tag{5.9}$$

and

$$v(\boldsymbol{x}) = V(\boldsymbol{x};\boldsymbol{\xi}^*), \quad \boldsymbol{x} \in \widetilde{\Omega} \cup \partial\widetilde{\Omega}, \tag{5.10}$$

where $\boldsymbol{\xi}^* = (3,0,0)$ is well-outside the solution domain $\widetilde{\Omega} = (0,1) \times (0,1) \times (0,1)$ and V is given by (5.4). We apply the boundary condition (4.5), (4.6) and (4.7), as in Section 4.1.

Figures 8 and 9 show the numerical solution for the real and imaginary parts of $u(x,1/2,1)$ and $v(x,1/2,1)$, $x \in [0,1]$, obtained using the MFS with $M = N = 2400$, $\eta = \eta_1 = 1.6$, $\eta_2 = 2$, in comparison with the exact solutions derived from (5.9) and (5.10). Clearly, excellent agreement between the numerical and exact solutions can be observed. In addition, in Figures 10 and 11 we present, respectively, the contours of the real parts of the exact solution u and approximation u_N, and the real parts of the exact solution v and approximation v_N, on the top face of the cube $[0,1] \times [0,1] \times \{1\}$. Again excellent agreement between the exact and numerical solutions is observed. Although not illustrated, it is reported that similar observations have been made for the corresponding imaginary parts.

6. Conclusions

In this paper, the MFS has been developed for solving the coupled system of diffusion–absorption equations governing optical fluorescence subject to Robin boundary conditions. The numerical results presented and discussed in both two and three dimensions confirm the accuracy of the numerical method employed. Furthermore, its meshless feature offers simplicity and ease of implementation for solving iteratively nonlinear inverse problems in forthcoming studies of optical fluorescence tomography. Note that the current study does not deal with implementational issues of the MFS such as the selection of the source points, the ill–conditioning of the MFS system and the potential difficulties in dealing with complex domains, as these are amply addressed in previous studies [3] and the recent book [5].

Acknowledgments

Fruitful discussions with A. Joshi and S. Arridge on the subject of fluorescence optical tomography are gratefully acknowledged.

References

[1] W. Bangerth and A. Joshi, *Adaptive finite element tomography for fluorescence optical imaging of tissue*, Inverse Problems, **24** (2008), Article ID 034011 (22 pages).
[2] S. Chandrasekhar, *Radiative Transfer*, Dover, New York, 1960.
[3] C.S. Chen, A. Karageorghis and Y. Li, *On choosing the location of the sources in the MFS*, Numerical Algorithms, **72** (2016), 107–130.

[4] C. S. Chen, S.-H. Shen, F. Dou and J. Li, *The LMAPS for solving fourth-order PDEs with polynomial basis functions*, Mathematics and Computers in Simulation, **177** (2020), 500–515.

[5] A. H-D. Cheng, C. S. Chen and A. Karageorghis, *An Introduction to the Method of Fundamental Solutions*, World Scientific, Singapore, 2025.

[6] G. Fairweather and A. Karageorghis, *The method of fundamental solutions for elliptic boundary value problems*, Advances in Computational Mathematics, **9** (1998), 69–95.

[7] F. Fedele, M. J. Eppstein, J. P. Laible, A. Godavarty and E. M. Sevick-Muraca, *Fluorescence photon migration by the boundary element method*, Journal of Computational Physics, **210** (2005), 109–132.

[8] A. Goravarty, D.J. Hawrysz, R. Roy, E. M. Sevick–Muraca and M. J. Eppstein, *Influence of the refractive index–mismatch of the boundaries measured in fluorescence–enhanced frequency–domain photon migration imaging*, Optics Express, **10** (2002), 650–653.

[9] J. C. Hauge and D. Crowdy, *A new approach to the complex Helmholtz equation with applications to diffusion wave fields, impedance spectroscopy and unsteady Stokes flow*, IMA Journal of Applied Mathematics, **86** (2021), 1287–1326.

[10] D. B. Ingham and L. C. Wrobel, *Boundary Integral Formulations for Inverse Analysis*, Computational Mechanics Publications, Southampton, 1997.

[11] A. Joshi, W. Bangerth and E. M. Sevick–Muraca, *Adaptive finite element based tomography for fluorescence optical imaging of tissue*, Optics Express, **12** (2004), 5402–5417.

[12] A. Joshi, W. Bangerth and E. M. Sevick–Muraca, *Non–contact fluorescence optical tomography with scanning patterned illumination*, Optics Express, **14** (2006), 6516–6534.

[13] A. Joshi, W. Bangerth, K. Hwong, J. Rasmussen and E. M. Sevick–Muraca, *Fully adaptive FEM based fluorescence optical tomography from time–dependent measurements with area illumination and detection fluorescence tomography with adaptive finite elements*, Medical Physics, **33** (2006), 1299–1310.

[14] A. Joshi, W. Bangerth, K. Hwong, J. Rasmussen and E. M. Sevick–Muraca, *Plane wave fluorescence tomography with adaptive finite elements*, Optics Letters, **31** (2006), 193–195.

[15] A. Karageorghis and C. S. Chen, *Multi-level method of fundamental solutions for solving polyharmonic problems*, Journal of Computational and Applied Mathematics, **456** (2025), 116220 (17 pages).

[16] A. Karageorghis, D. Lesnic and L. Marin, *A survey of applications of the MFS to inverse problems*, Inverse Problems in Science and Engineering, **19** (2011), 309–336.

[17] J. Lin, C. S Chen and C.-S. Liu, *Fast solution of three dimensional modified Helmholtz equations by the method of fundamental solutions*, Communications in Computational Physics, **20** (2016), 512–533.

[18] A. B. Thompson and E. M. Sevick–Muraca, *Near–infrared fluorescence contrast–enhanced imaging with intensified charge–coupled device homodyne detection: measurement precision and accuracy*, Journal of Biomedical Optics, **8** (2003), 111–120.

[19] D. Wang, C. S. Chen and W. Li, *An efficient MAPS for solving fourth order partial differential equations using trigonometric functions*, Computers and Mathematics with Applications, **79** (2020), 934–946.

[20] G. Yao, C. H. Tsai and W. Chen, *The comparison of three meshless methods using radial basis functions for solving fourth–order partial differential equations*, Engineering Analysis with Boundary Elements, **34** (2010), 625–631.

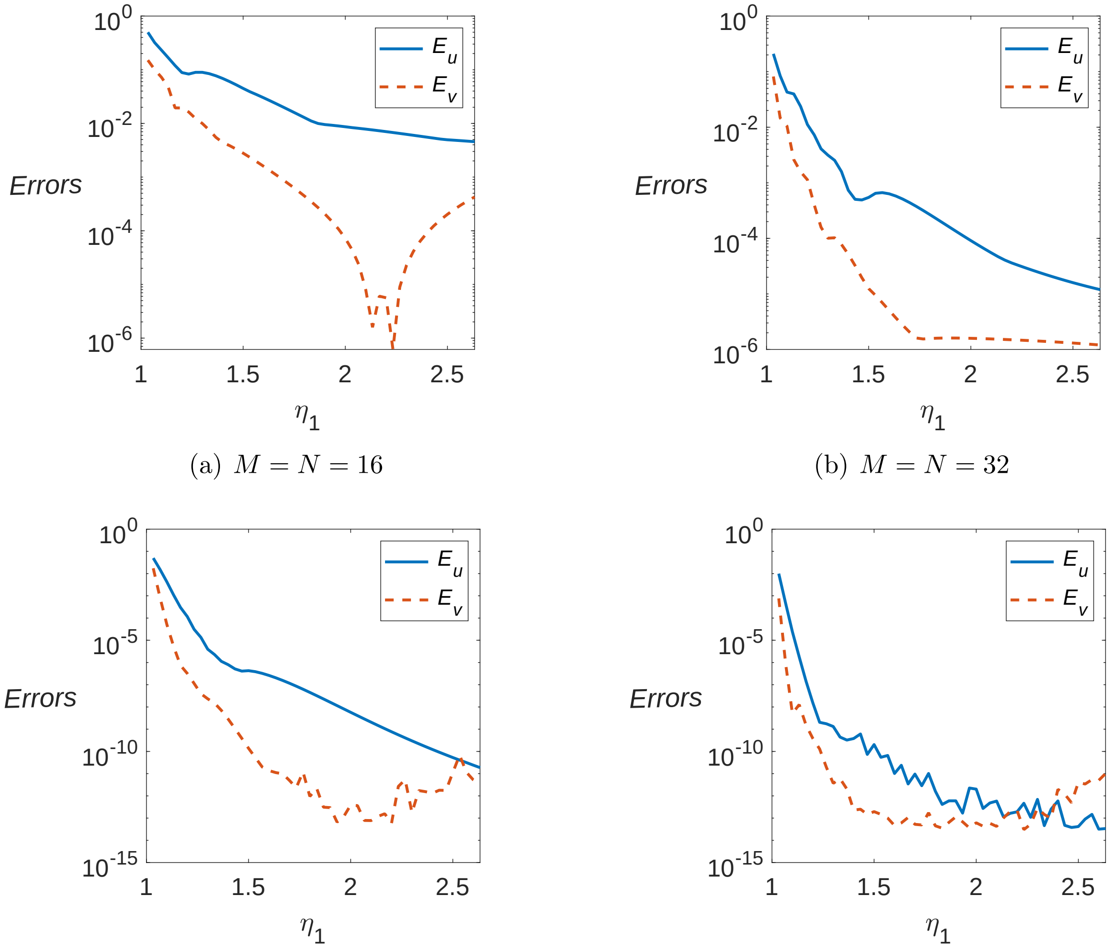

(a) $M = N = 16$ (b) $M = N = 32$

(c) $M = N = 64$ (d) $M = N = 128$

FIGURE 1. Errors E_u and E_v with varying η_1 (and η_2) for different $M = N$.

DEPARTMENT OF MATHEMATICS AND STATISTICS, UNIVERSITY OF CYPRUS/ ΠΑΝΕΠΙΣΤΗΜΙΟ ΚΥΠΡΟΥ, P.O.BOX 20537, 1678 NICOSIA/ΛΕΥΚΩΣΙΑ, CYPRUS/ΚΥΠΡΟΣ
E-mail address: `andreask@ucy.ac.cy`

DEPARTMENT OF APPLIED MATHEMATICS, UNIVERSITY OF LEEDS, LEEDS LS2 9JT, UK
E-mail address: `amt5ld@maths.leeds.ac.uk`

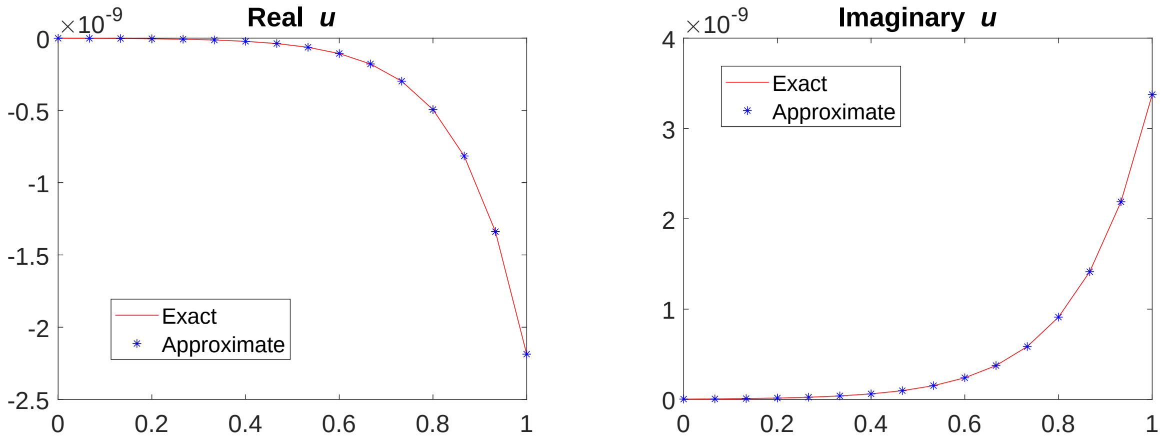

(a) Real (b) Imaginary

FIGURE 2. Real and imaginary parts of numerical and exact solutions for $u(x, 1)$ with $x \in [0,1]$ on top boundary $y = 1$.

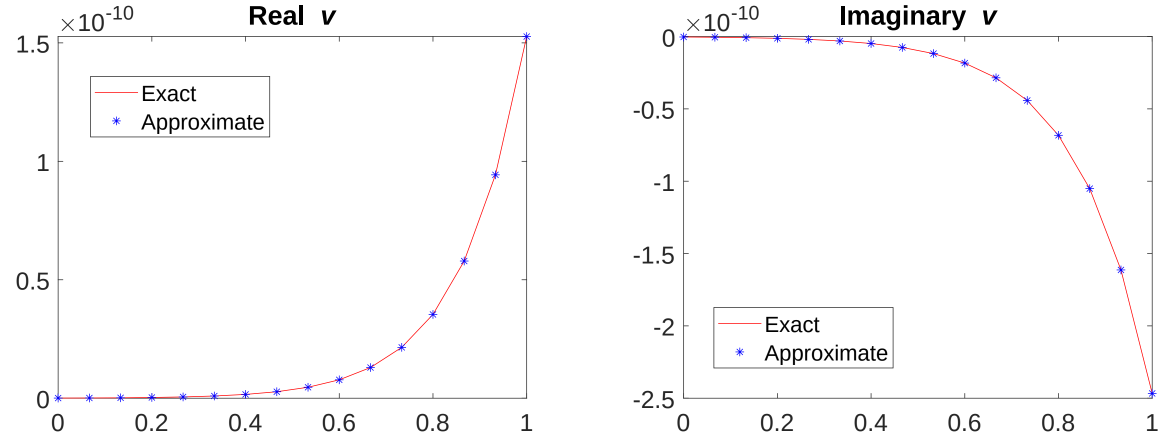

(a) Real (b) Imaginary

FIGURE 3. Real and imaginary parts of numerical and exact solutions for $v(x, 1)$ with $x \in [0,1]$ on top boundary $y = 1$.

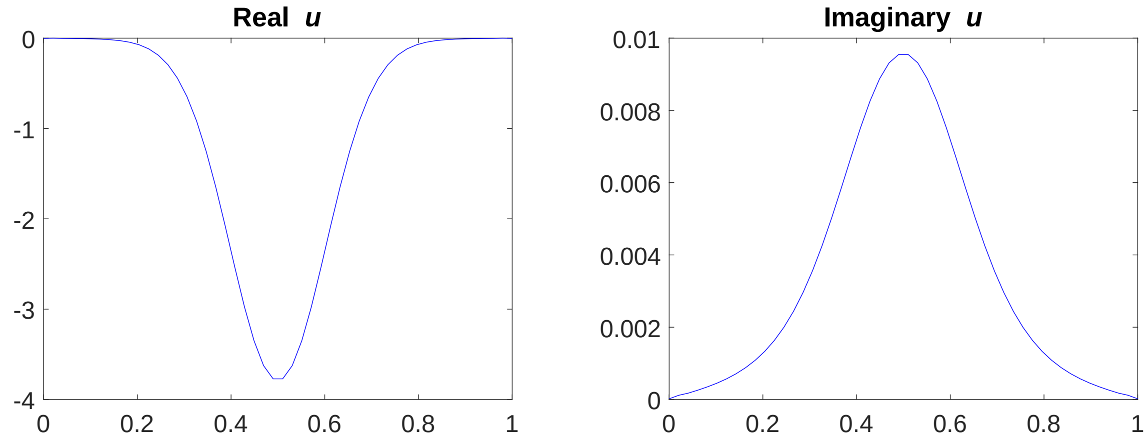

(a) Real (b) Imaginary

FIGURE 4. Real and imaginary parts of numerical solution for $u(x, 1)$ with $x \in$ [0,1] on top boundary $y = 1$, for the physical problem.

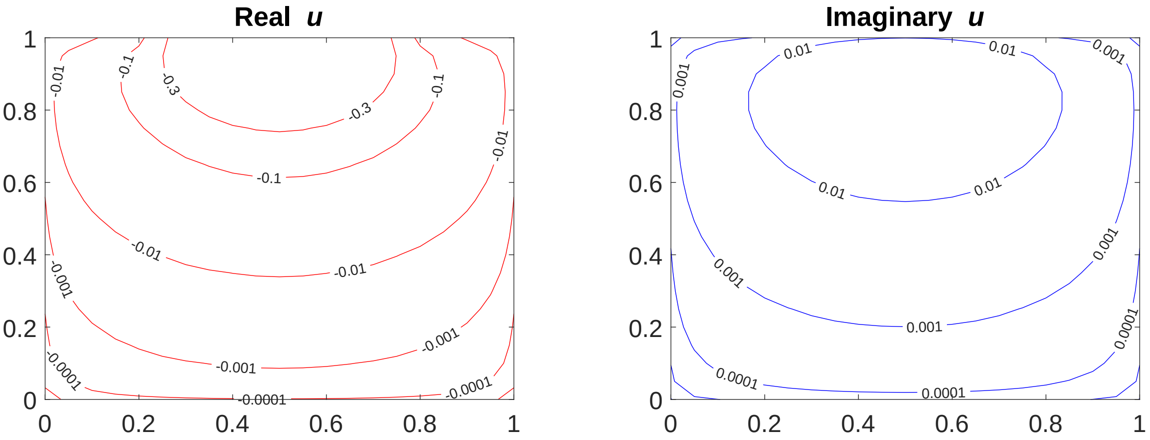

(a) Real (b) Imaginary

FIGURE 5. Real and imaginary parts of numerical solution for $u(x, y)$ with $(x, y) \in \widetilde{\Omega} \cup \partial\widetilde{\Omega} = [0, 1] \times [0, 1]$, for the physical problem.

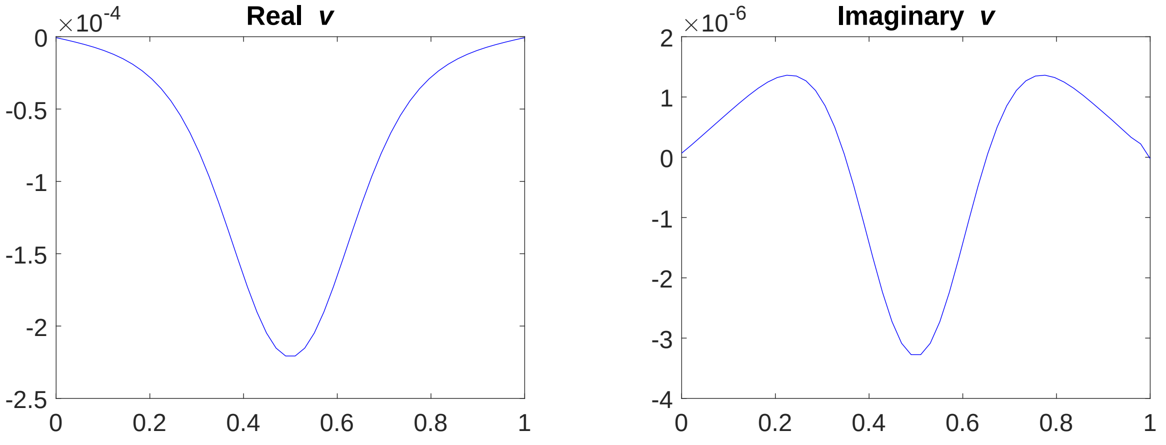

(a) Real (b) Imaginary

FIGURE 6. Real and imaginary parts of numerical solution for $v(x,1)$ with $x \in$ [0,1] on top boundary $y = 1$, for the physical problem.

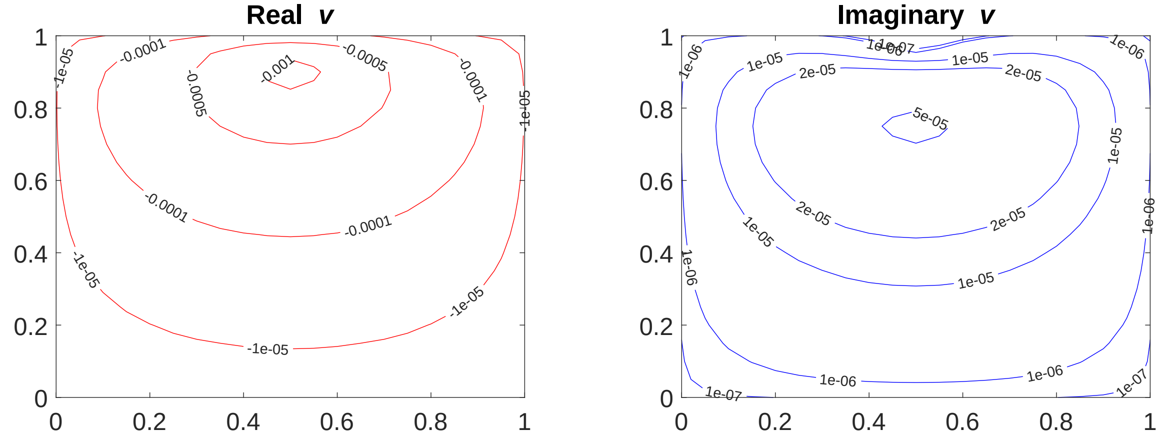

(a) Real (b) Imaginary

FIGURE 7. Real and imaginary parts of numerical solution for $v(x,y)$ with $(x,y) \in \widetilde{\Omega} \cup \partial\widetilde{\Omega} =$ [0,1] [0,1], for the physical problem.

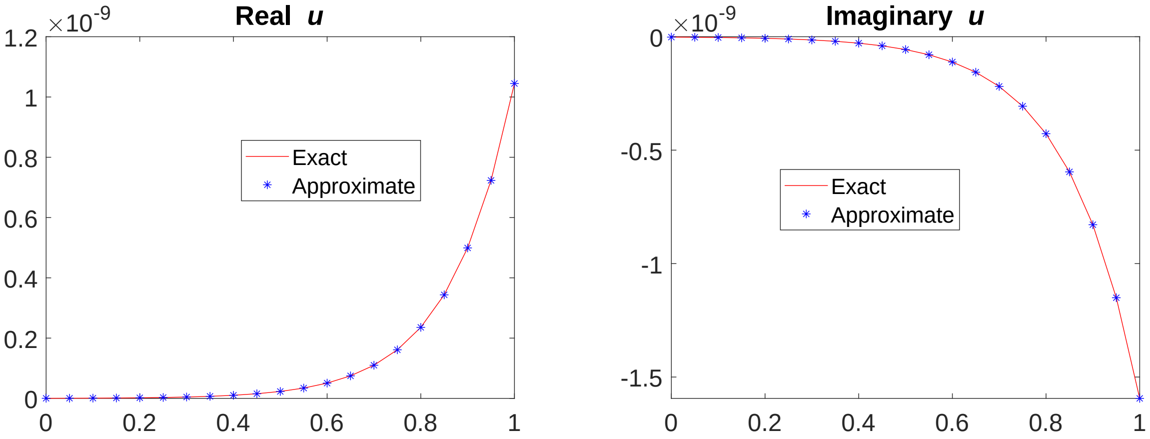

(a) Real (b) Imaginary

FIGURE 8. Real and imaginary parts of numerical and exact solutions for $u(x, 1/2, 1)$ with $x \in$ [0,1] on top face $z = 1$ and $y = 1/2$.

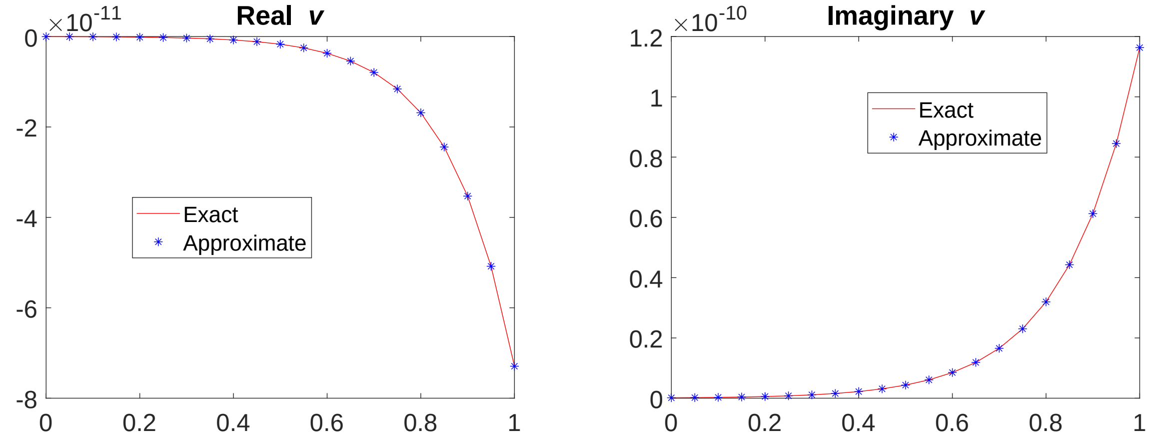

(a) Real (b) Imaginary

FIGURE 9. Real and imaginary parts of numerical and exact solutions for $v(x, 1/2, 1)$ with $x \in$ [0,1] on top face $z = 1$ and $y = 1/2$.

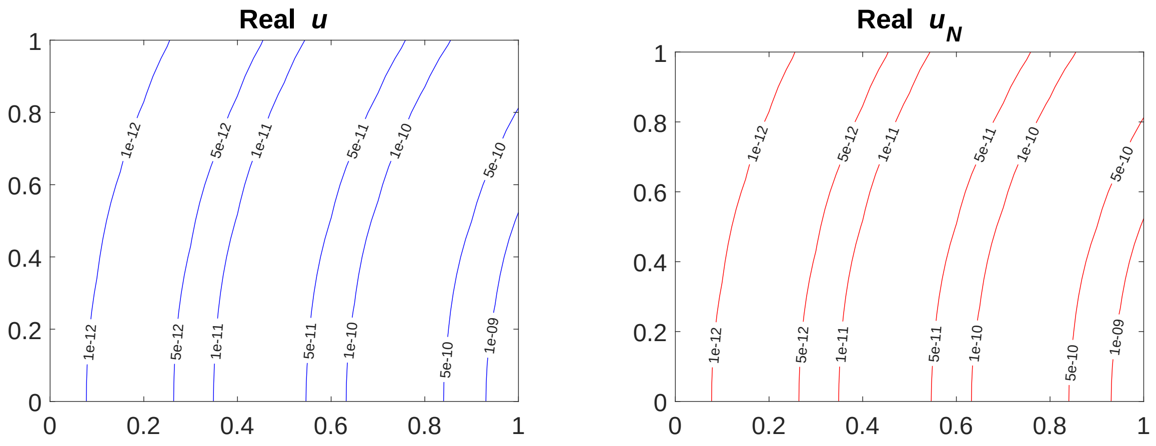

(a) Exact (b) Approximate

FIGURE 10. Real parts of numerical and exact solutions for $u(x, y, 1)$ with $(x, y) \in [0, 1] \times [0, 1]$, on top boundary $z = 1$.

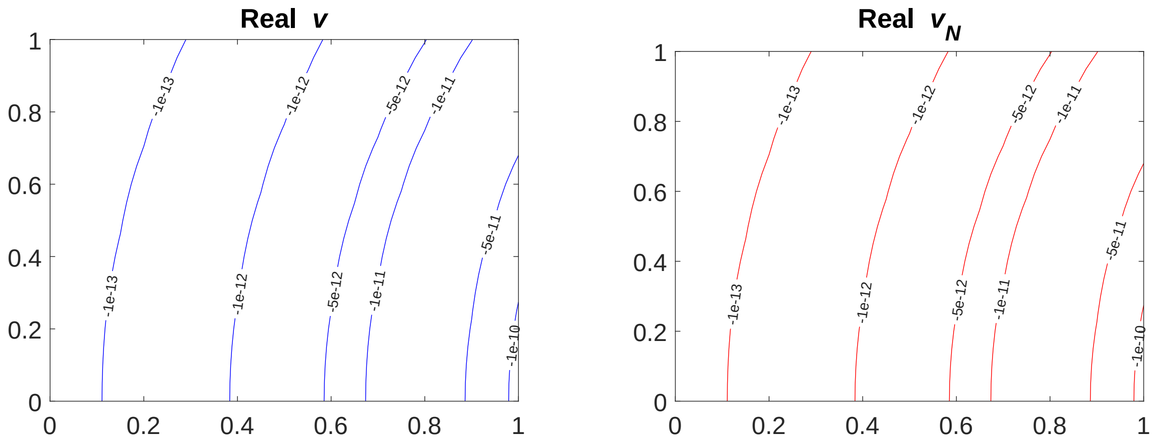

(a) Exact (b) Approximate

FIGURE 11. Real parts of numerical and exact solutions for $v(x, y, 1)$ with $(x, y) \in [0, 1] \times [0, 1]$, on top boundary $z = 1$.